Generation of energetic negative ions from clusters using intense laser fields

2013 New J. Phys. 15 043036

(http://iopscience.iop.org/1367-2630/15/4/043036)

New Journal of Physics
The open access journal for physics

Generation of energetic negative ions from clusters using intense laser fields

R Rajeev, T Madhu Trivikram, K P M Rishad, V Narayanan and M Krishnamurthy[1]

Tata Institute of Fundamental Research, 1, Homi Bhabha Road, Mumbai 400 005, India
E-mail: mkrism@tifr.res.in

New Journal of Physics **15** (2013) 043036 (16pp)
Received 30 December 2012
Published 19 April 2013
Online at http://www.njp.org/
doi:10.1088/1367-2630/15/4/043036

Abstract. Intense laser fields are known to induce strong ionization in atoms. In nanoclusters, ionization is only stronger, resulting in very high charge densities that lead to Coulomb explosion and emission of accelerated highly charged ions. In such a strongly ionized system, it is neither conceivable nor intuitive that energetic negative ions can originate. Here we demonstrate that in a dense cluster ensemble, where atomic species of positive electron affinity are used, it is indeed possible to generate negative ions with energy and ion yield approaching that of positive ions. It is shown that the process behind such a strong charge reduction is extraneous to the ionization dynamics of single clusters within the focal volume. Normal and well-known charge transfer reactions are insufficient to explain the observations. Our analysis reveals the formation of a manifold of Rydberg excited clusters around the focal volume that facilitate orders of magnitudes more efficient electron transfer. This phenomenon, which involves an active role of laser-heated electrons, comprehensively explains the formation of copious accelerated negative ions from the nano-cluster plasma.

[1] Author to whom any correspondence should be addressed.

Contents

1. Introduction 2
2. Experiment 3
3. Results and discussion 5
Acknowledgments 14
References 15

1. Introduction

The extreme nonlinear, non-perturbative physics involving the interaction of intense ultrashort laser pulses with matter is known to effectively ionize atoms to very high charge states [1–3]. At intensities beyond $10^{12}\,\mathrm{W\,cm^{-2}}$ most atoms undergo multiphoton ionization [4], while over the barrier ionization is imminent beyond $10^{14}\,\mathrm{W\,cm^{-2}}$ in almost all atomic systems [5]. Augmenting the field-ionization processes is collisional ionization by laser-heated electrons to form a hot dense plasma [6] especially in dense systems, such as solids or nanoclusters [1]. In particular, with nanoscale clusters, ionization is even more enhanced, generating ions charged as high as Xe^{45+} in Xe clusters [7]. Even at moderate intensities of $10^{16}\,\mathrm{W\,cm^{-2}}$, Ar clusters are known to generate more than 60% of the atoms in charge states larger than 7+ [8]. Clusters with such high charge densities expand under Coulomb and hydrodynamic pressures to accelerate ions to energies upto MeV [9]. It is only these characteristic features of immense ionization and ion acceleration that has attracted interest in all the experimental [8, 10, 11] and theoretical explorations [1, 2] on nanoclusters so far. It is non-intuitive that from such hot, dense and highly ionized matter, negative ions with kinetic energies of a few hundreds of keVs can originate.

Theoretical investigations on the role of the inverse process of ionization, namely recombination, within clusters has recently been performed [12]. However, estimates [13] predict negligible charge reduction within the nanoplasma and do not favor generation of negative ions. On the experimental front, explorations on the formation of negative ions in intense laser fields have been limited both by the nature of the diagnostics used to probe the ion emission and by the choice of the target system. A large number of the experiments pertaining to cluster ionization so far have relied on the measurements of time-of-flight of ions at low inter-cluster densities $\rho_C \sim 10^{10-11}\,\mathrm{clusters\,cm^{-3}}$ using skimmed cluster beams under the conditions of a large mean free path. Since in these cases, only positive atomic ions are expected, the measured arrival time is used to interpret the charge-integrated ion energy distributions [14]. Resolving and discriminating high-energy negative ions, however, necessitates the use of a charge and energy resolving ion spectrometer such as a Thomson parabola ion imaging spectrometer (TPS) [11]. Although TPS has successfully been used to explore the dynamics of cluster ionization, these studies were limited to cluster systems that comprised atoms/molecules [8, 11] that do not have positive electron affinity, and hence negative ion formation is not considered. Moreover, the interaction environment in these experiments involved the so-called single-cluster regime where isolated cluster explosions are probed. Studies on the change in ion charge states after the Coulomb explosion from single clusters due to dense cluster ensemble of clusters have never been reported. Experiments that involve inter-cluster collisions would need higher cluster densities, $\rho_C > 10^{12}\,\mathrm{clusters\,cm^{-3}}$, which is possible by sampling a dense ensemble of clusters immediately at the throat of the

supersonic nozzle. However, such studies predominantly concentrated on the measurement of k-shell x-ray photons [15] or fusion neutrons [16]. The presence of highly charged ions was only inferred through high-resolution x-ray spectroscopy [17] and not by direct ion measurements. Recently, however, ion spectrometry was explored very close to the nozzle, but with droplets that are a few hundred times larger than nm clusters. Experiments with 0.3 μm droplets of CO_2 have shown that C^- ions up to 600 keV [18] are formed at 10^{17} W cm^{-2}. Coulomb implosion was invoked to explain the emission of the high-energy negative ions. While a detailed mechanism of the acceleration of negative ion was discussed, the very process that generates the negative ions was not elaborated. In a more recent experiment [19], irradiation of a water spray jet with a droplet size of 1 μm at 10^{19} W cm^{-2} was found to generate O^- ions, and charge transfer was argued to be responsible for the formation of accelerated O^-.

We demonstrate here the generation of hot negative ions from much smaller clusters (< 10 nm) that seems contrary to the expected ion emission features from small clusters. Our study reveals that a dense ensemble of laser-irradiated nanoclusters collectively forms a very efficient system for reducing the charge on Coulomb exploded ions with no loss of kinetic energy. Negative ion generation is shown to be a strong function of the cluster ensemble density (ρ_C). At large ρ_C ($> 10^{12}$ clusters cm^{-3}), negative ions are observed, with clear signatures of O^- and a smaller fraction of C^-, while no trace of negative ions are found at lower cluster density ($\rho_C \sim 10^{11}$ clusters cm^{-3}). Further, at $\rho_C \sim 10^{14}$ clusters cm^{-3}, the signal strength and kinetic energy of O^- are comparable to O^+. The absence of any negative ion signal from single isolated clusters suggests that intra-cluster mechanisms, such as Coulomb implosion [18], are not dominant in small clusters (of a few nm). Besides, our analysis reveals that the obvious mechanisms of charge reduction, electron recombination (ER) and normal charge transfer [19] fail to explain the large fraction of negative ions observed in measurements. We show that it is the electronic excitations in the hot dense plasma that is responsible for the large yield of negative ions.

Although heat transport by electrons from the focal zone has been probed earlier [20], the consequence of this for the neighboring atoms and their influence on the ion particle emission have not been investigated. We show that streaming electrons from the focal volume have optimum energy to electronically excite clusters beyond the focal volume. Accelerated highly charged ions that encounter charge transfer collisions with the excited clusters are reduced very effectively due to an enhanced charge transfer cross section. The extent of such an influence is strongly dependent on the ensemble cluster density. In this paper, a detailed study is conducted to comprehensively address the negative ion formation from a strongly ionized plasma, and a very efficient plasma-assisted mechanism of electron transfer involving Rydberg excited clusters outside the focal volume is presented.

2. Experiment

We use a supersonic jet system coupled to a state-of-the-art TPS developed recently [11] in two varied experimental geometries for measuring ionization from single isolated clusters at low ensemble density (figure 1(a)) and also at high cluster densities (figure 1(b)). Briefly, $(CO_2)_n$ clusters are produced with a supersonic jet fitted with a 750 μm conical nozzle of 45°. Cluster generation in these experiments is characterized by Rayleigh scattering measurements [21] in conjunction with Hagena's scaling laws [22] and are known to produce clusters with log normal size distribution [23] where the mean value of the distribution is controlled by the stagnation

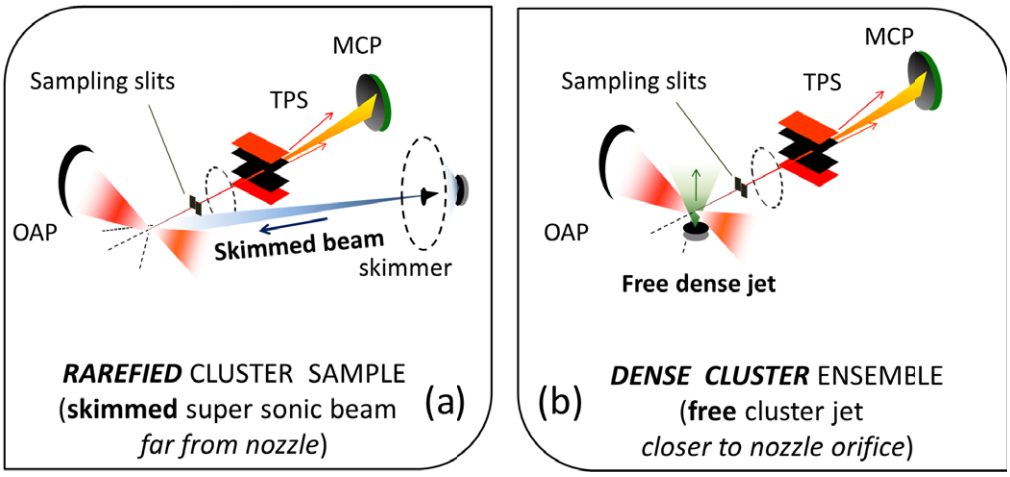

Figure 1. Experimental geometries for (a) probing single-cluster explosion dynamics ($\rho_C \sim 10^{11}$ clusters cm^{-3}) and (b) exploring multi-cluster effects in a densely clustered medium ($\rho_C \sim 10^{12}$–10^{-14} clusters cm^{-3}). The laser focus in (a) is 300 mm downstream of the nozzle and in (b) is 6–100 mm downstream of a free jet. The skimmed beam in (a) has a beam span of 10 mm, while the free jet assumes a natural jet span. The focus–nozzle distance in the free jet in (b) can be varied to change the cluster density ρ_C.

pressure on the nozzle. At a stagnation pressure of 10 atm, we decipher the generation of $(CO_2)_n$ clusters with a mean value of $\langle n \rangle = 36\,000$. High cluster density ($\rho_C > 10^{12}$ clusters cm^{-3}) experiments are performed focusing the laser pulses at 6–100 mm downstream of the nozzle (figure 1(b)) on a free expanding jet. On the other hand, to decipher ionization in single isolated clusters at low density ($\rho_C \sim 10^{11}$ clusters cm^{-3}), the laser pulses are focused at the exit of a skimmer placed about 300 mm away from the nozzle on the axis of the supersonic jet. Differential pumping ensured that even with the gas load, the chamber pressure in the cluster source chamber is maintained at 10^{-4} Torr and the chamber at the exit of the skimmer is maintained at less than 10^{-6} Torr. In both the geometries, the focus and the TPS axis are fixed. The density in the free jet experiment is varied by changing the distance between the supersonic jet source and the laser focus. The supersonic jet nozzle system is set up on a translational stage and is moved away from the focal spot. The skimmed beam and the dense jet experimental geometries are realized independently, allowing for easy switching between the configurations.

The ultrashort intense laser pulses used in these experiments are from a chirp pulse amplification laser system that generates 40 fs pulses centered at 806 nm, with 300 mJ pulse energy at 10 Hz repetition rate. In these experiments, we use about 50 mJ pulses focused with an off-axis parabolic mirror to generate intensities up to 10^{17} W cm^{-2}. Perpendicular to the direction of the laser and the supersonic jet, we use the TPS to probe the ions generated in the focal volume. The spectrometer is designed to give the best possible charge state resolution for the use of extended targets such as clusters [11]. We use a pair of movable knife edges to dynamically restrict the focal zone sampled in addition to a 300 μm ion extraction aperture placed at about 30 cm from the focal point of the laser. The cluster jet is much larger than the Rayleigh range of the laser focus, so ion generation from the pre-focal and post focal zones is inevitable and ions generating from these areas should be discriminated to achieve a good charge

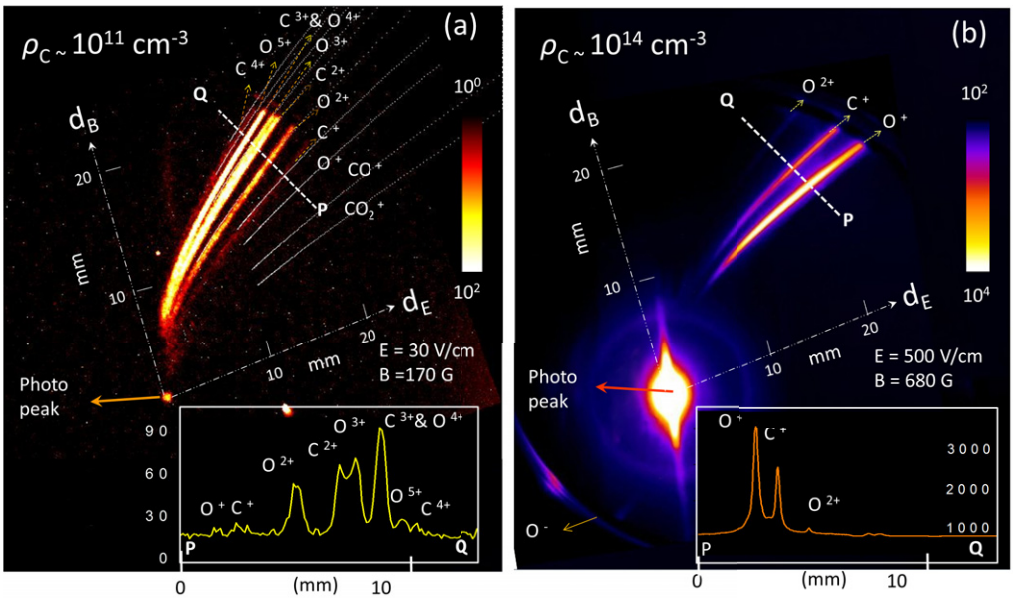

Figure 2. (a) Thomson parabola (TP) image of positive ions emitted from $(CO_2)_n$ ($\langle n \rangle = 36\,000$) at 2×10^{16} W cm^{-2} and a density ρ_C of about 10^{11} clusters cm^{-3} measured on the skimmed beam geometry in figure 1. The inset shows a one-dimensional profile of the image along the line PQ. (b) A similar TP image of positive ions from $(CO_2)_n$ ($\langle n \rangle = 36\,000$) but measured at the exit of the supersonic jet nozzle at 10^{13} cm^{-3} cluster density (figure 1(b)). The signal at the origin is due to the scatter light and x-rays generated at the focal point. A faint ring that appears around the origin is due to the diffraction of the scatter light from the 100 μm aperture. Note that the faint signal in the diametrically opposite quadrant (labeled O^-) show the presence of energetic negative ions. The image in figure 2(a) is the result of averaging over 40 000 laser shots, while the image in figure 2(b) was arrived at by averaging 3000 laser shots. d_E and d_B are electric and magnetic drifts, respectively. The E and B fields indicated are chosen so as to maintain the E/B^2 ratio, which conserves the curvature of the parabolic traces.

resolution [11]. Sampling a restricted interaction volume not only improves the resolution but also avoids longitudinal intensity convolution in the ion measurements. The electric field for the TPS is due to a pair of electrodes of 80 × 40 mm separated by 10 mm and the magnetic field is applied using a pair of permanent magnets placed 1 cm away on each side of the electrodes. Parabolic traces of the ions are detected using a pair of 40 mm micro-channel plates coupled to a phosphor screen and imaged using a CCD camera.

3. Results and discussion

The contrasting features of ion emission from CO_2 clusters in the single-cluster regime measured at ρ_C of 10^{11} cm^{-3} (figure 2(a)) and in a densely clustered media at ρ_C of 10^{13} cm^{-3} (figure 2(b)) are presented here for a direct comparison. The intensity within the sampled

interaction zone in both cases is 2×10^{16} W cm^{-2} and the average cluster size is $\langle n \rangle \sim 36\,000$. It is to be noted that a skimmed beam is not just a low dense zone but is also restricted in the beam span (10 mm in this case) as against the natural span of a free jet. We use the standard equations for ion traversal in the parallel electric (E) and magnetic (B) fields of the TPS to simulate the ion trajectories [11] and these are represented by the dotted lines in figure 2(a) for the different ionic and molecular fragments of the CO_2 system, superposed on the measured TP image. In conformity with the expectations from experiments performed over a decade using much simpler time-of-flight methods [1], we see positive atomic ions of C and O with the higher charge states having large kinetic energies (parabolic trace extends closer to the origin). Low cluster density ($\sim 10^{11}$ cm^{-3}) ensures a large mean free path that is devoid of inter-cluster effects and thus the measured traces are a clear reflection of ionization dynamics of single isolated clusters. Equipped with an improved resolution, the spectrometer [11] resolves ion traces with very close values of m/q. The line cut of the well-resolved traces is plotted in the inset of figure 2(a). It also shows that the spectrum is devoid of any measurable signal from high-energy (> 5 keV) positive molecular ions (CO_2^+ and CO^+). The dotted parabolic lines show the region over which these ions are expected to be seen if they are observed in the cluster explosion.

Our efforts to directly measure the ion spectrum in the high cluster density regime ($> 10^{13}$ clusters cm^{-3}) with the clusters of a similar size and at the same laser intensity yielded an image that is very different. As seen in figure 2(b), in dense cluster ensemble experiments we do not find any highly charged ions and the spectrum is dominated only by C^+ and O^+, which were negligibly small in figure 2(a). The inset shows a line cut of the parabolic image showing the presence of predominantly singly charged ions. In Coulomb explosion of clusters it is expected that the low charge state (if they exist) have low energy and the high charge states have high energy. Contrary to this expectation, in figure 2(b) we have low charge state ions of high kinetic energy (parabolic traces corresponding to C^+ and O^+ in figure 2(b) extend very close to the origin). Inter-cluster interaction at high density appears to have reduced the highly charged ions with very little change in the kinetic energy and hence we have O^+ and C^+ ions with high kinetic energy. In fact, the charge reduction seems to go even further; in figure 2(b) we see a small trace of parabola in the direction diametrically opposite to the positive ion traces, indicating the presence of even negative ions. We reverse the bias of the voltage applied on the electrodes and the polarity of the applied magnetic fields to disperse the negative ions on the major portion of the detector. The resultant TP image, under otherwise similar experimental conditions and interaction parameters, is shown in figure 3(a). We see a clear signature of O^- and C^- ions. In addition to the fact that there are two O atoms per CO_2 molecule, O^- is the dominant negative ion, presumably because of a much larger electron affinity of O [24]. Negative ion signal is detected only under high cluster densities (see figures 3(b) and (c)) and the fact that this is accompanied by high-energy low charge state ions (C^+ and O^+) seems to suggest very strongly that this is not an intracluster process but an effect of inter-cluster interactions.

To probe this further, we measure the change in negative ion signal propensity with cluster density. Figures 4(d)–(f) show that the O^- signal strength increases strongly with the cluster density. The corresponding positive ion traces measured by reversing the polarity of the E and B fields are shown in figures 4(a)–(c). Further, the energy of the negative ions can be tuned with cluster size by varying the backing pressure of the jet [25]. In figure 5, we show the TP image measured as a function of cluster size. An increase in the O^- energy (traces extend close to the origin) and yield is seen much the same way as is expected for positive ions. Figure 6(a) shows the normalized kinetic energy spectrum of the O^+ and O^- ions derived from the parabolic traces

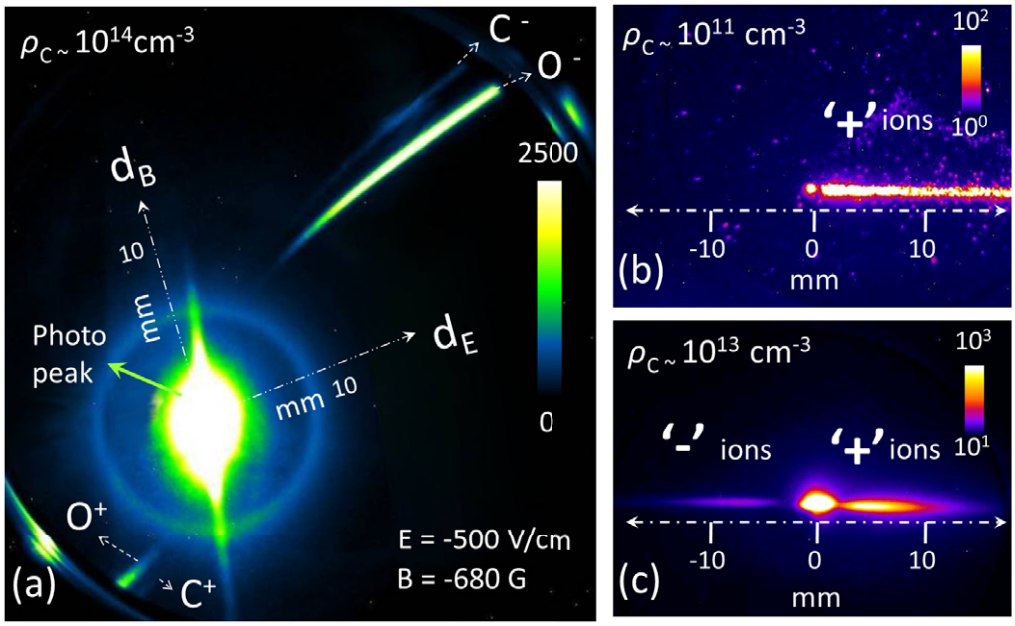

Figure 3. (a) TP image of $(CO_2)_n$ ($\langle n \rangle = 36\,000$) at 2×10^{16} W cm^{-2} measured at a cluster density of about 10^{14} cm^{-3} (same as in figure 2(a)) but with reversed E and B fields. Signal at the origin is due to the scatter light and x-rays generated at the focal point. A faint ring that appears around the origin is due to the diffraction of scatter light from the 100 μm aperture. d_E and d_B are electric and magnetic drifts, respectively. (b) Ion image obtained at ρ_C of 10^{11} cm^{-3} with only electric field applied. Positive ions are deflected toward right and negative ions, if any, on the left side. (c) Ions deflected by electric field deflection (as in (b)) but at a higher $\rho_C \sim 10^{13}$ cm^{-3} show negative ions on the left side.

for oxygen shown in figures 4(a)–(f), respectively, at various cluster densities ρ_C. As can be seen, the yield and the energy O^+ and O^- are comparable at $\rho_C \sim 10^{14}$ cm^{-3}. Figure 6(d) shows the O^- energy derived from the TP images and the inset shows that the maximum ion energy increases with the cluster size or stagnation pressure. The fact that the maximum negative ion energy can be tuned with cluster size much like that of positive ions validates that the origin of negative ions is positive ions from exploding clusters.

What is the underlying physics of O^- generation with a signal strength comparable to O^+? First, we consider the possibility of the Coulomb implosion mechanism proposed in much larger (300 nm) CO_2 clusters [18]. Their observations seem to indicate only the presence of C^- ions. It is not clear why the O^- ions that may be expected to dominate are not present. Further, this mechanism would also imply negative ion formation even from single isolated clusters. We probed hard to look for negative ions at low cluster density (10^{11} cm^{-3}) and failed to see any measurable signal. Even if the negative ion signal was 2–3 orders of magnitude smaller than that observed at high density, it would be measurable in our spectrometer. Figure 3(b) shows the signal on the detector with only electric field applied such that the dispersion is only on one axis and positive ion signal is differentiated from the negative ions. Since the ions are dispersed on a single dimension, the signal strength required for unambiguous identification of the presence of negative ions is smaller. However, we do not see any measurable negative ions in figure 3(b)

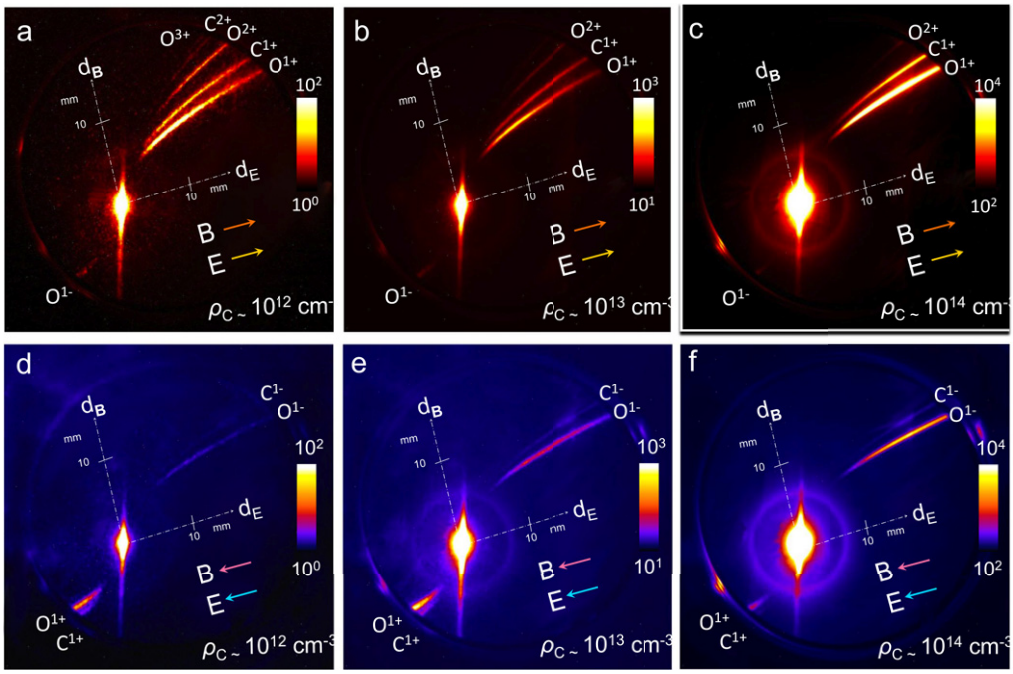

Figure 4. (a) TP image of $(CO_2)_n$ ($\langle n \rangle = 36\,000$) at 2×10^{16} W cm^{-2} and different cluster densities. d_E and d_B are electric and magnetic drifts, respectively. Panels (a)–(c) have positive ion traces in the top right quadrant while panels (d)–(f) are images with reversed bias and hence negative ions are in the top right quadrant.

in the direction opposite to those of positive ions. The absence of any negative ion signal from single isolated clusters (see figure 3(b)) and the density dependence of negative ion formation (figures 4(c)–(e)) suggest that intra-cluster mechanisms (such as the Coulomb implosion [18]) are not dominant processes at least in small clusters (of a few nm). It should also be noted that the large positive charge densities within nanoplasma form a strong electrostatic field that could re-ionize any anions formed from a single cluster and make their origin from a single isolated cluster plasma questionable.

We explore an other well-known method of generating negative ions, the dissociative electron attachment (DEA) [26]. Attachment of low-energy electrons to molecular systems has many orders of magnitude larger cross section than that of atoms [27] and negative molecular ions dissociate to form atomic negative ions. The presence of the cold electron swarm in a densely clustered media [28] could, in principle, bring this mechanism as a viable option. However, in order for DEA with molecular ions to be possible for forming high-energy O^- or C^-, it is necessary to observe high-energy molecular ions from the clusters. In the positive ion TP spectrum measured from isolated clusters, shown in figure 2(a), we do not see any measurable signal of molecular ions of high energy (larger than 5 keV) and this rules out the possibility of generating negative ions via DEA with molecules.

To comprehend these results, we take the cue from two major observations summarized in figure 6. Firstly, it is clear from figure 6(a) that the inter-cluster density is a crucial tuning parameter in the generation of negative ions. The strong dependence of the negative ion yield

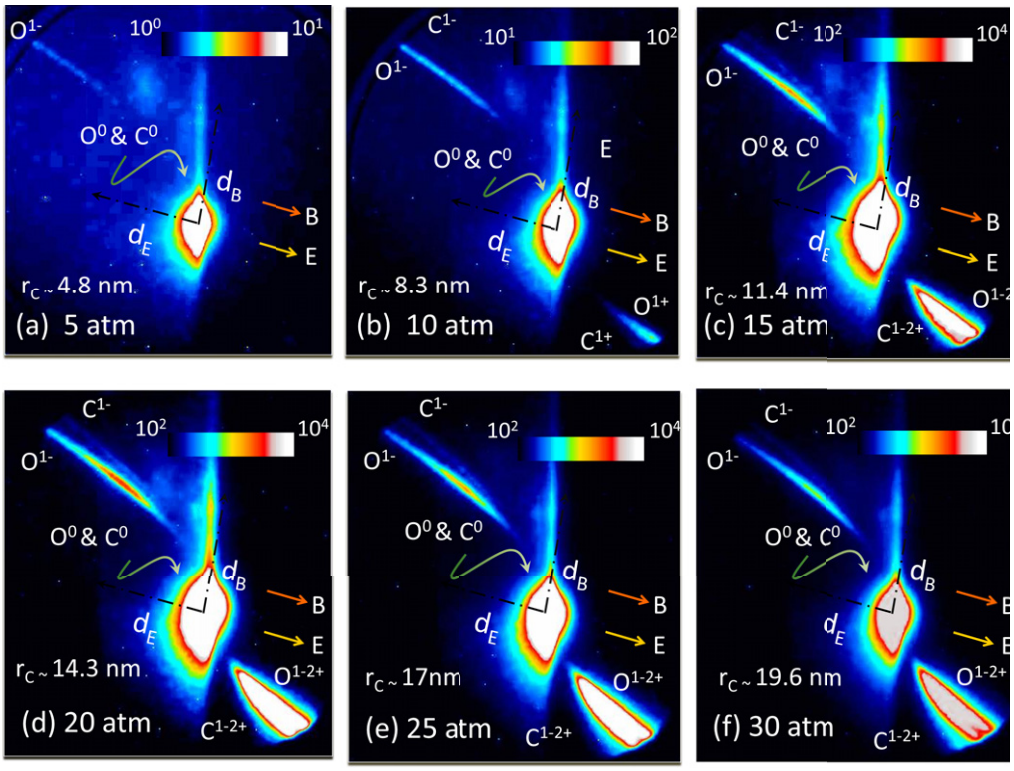

Figure 5. (a) TP image of $(CO_2)_n$ ($\langle n \rangle = 5000$–$65\,000$) at 2×10^{16} W cm^{-2} and different stagnation chamber pressures (5–30 atm). r_C is the radius of clusters produced at a given backing pressures. All measurements were done at 6 mm downstream the nozzle. d_E and d_B are electric and magnetic drifts, respectively.

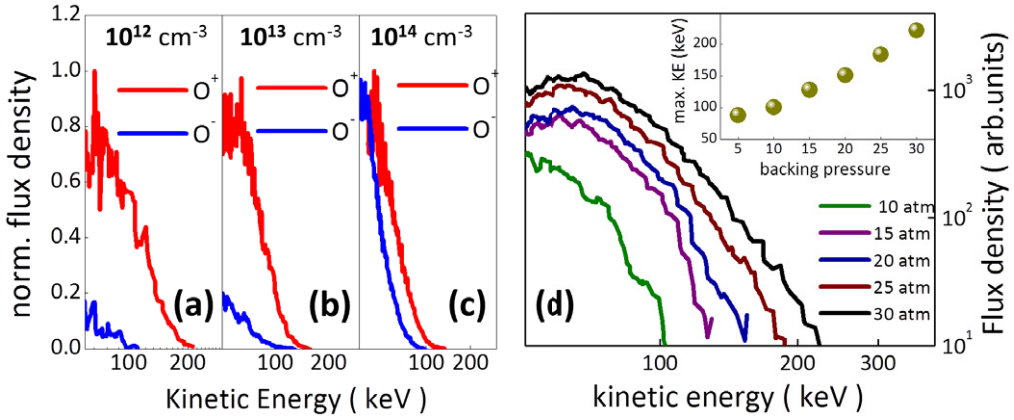

Figure 6. (a)–(c) Normalized kinetic energy spectrum of O^- and O^+ ions determined from the TP images (given in figure 4) at various cluster densities. (d) Kinetic energy spectrum of O^- ions for different cluster sizes changed by increasing the backing pressure on the nozzle (TP images are shown in figure 5). Inset shows the maximum energy of the distribution plotted as a function of the stagnation pressure. Cluster sizes for these pressures are as indicated in figure 5.

on the cluster density suggests that negative ion formation is extraneous to the single-cluster ionization dynamics and involves multi-cluster effects. Secondly, the fact that the spectral features of the negative ions are similar to those of positive ions and the increase of negative ion kinetic energy with cluster size suggest that the force driving the acceleration is verily the Coulomb explosion of positively charged nanoclusters. The scenario for the generation of negative ions as it appears can thus be summarized as a two-step process. In the first step, the clusters are ionized by the interaction of the intense ultrashort pulse. In the second step, accelerated ions ejected from the nanoclusters in the focal volume traverse through the medium surrounding the focal volume and are charge reduced.

The basic processes that reduce the charge of an ion A^{q+} are

$$A^{q+} + M \rightarrow A^{(q-k)+}, \tag{1}$$

$$A^{q+} + e \rightarrow A^{(q-1)+}. \tag{2}$$

The first process is the capture of bound electrons from a target atom/molecule/cluster (termed M) in a collision and is generally termed as a charge transfer reaction. The cross section for the reaction varies with the center of mass collision energy and the single electron transfer ($k = 1$) cross sections are larger than multiple electron capture ($k > 1$). The electron donor (M) can be in the ground state or in an excited state. The second process, termed as the ER reaction, happens when a free electron is captured by an ion. The ER reactions can occur in mainly three different ways:

$$\text{Radiative recombination:}\quad A^{q+} + e \rightarrow A^{(q-1)+*} \rightarrow A^{(q-1)+} + h\nu. \tag{3}$$

$$\text{Dielectric recombination:}\quad A^{q+} + e \rightarrow A^{(q-1)+**}, \tag{4}$$

$$\text{Triple recombination:}\quad A^{q+} + 2e \rightarrow A^{(q-1)+} + e. \tag{5}$$

In radiative recombination, ions capture the free electron and the radiative loss of excess energy results in the formation of the charge reduced ion. In dielectric recombination, the free electron is captured to high-lying bound states and the excess energy is dielectronically coupled to excite an inner electron into a higher bound state. The doubly excited states lose energy in collisions or by photo emission. They are also prone to auto-ionization. At high electron density, triple recombination occurs when two electrons simultaneously interact with the ion. One electron is captured in the process and the other is scattered to carry away the excess energy. The cross section for these mechanisms are different and depend on the electron energy and density. However, it is possible to obtain an effective recombination cross section for a given electron density and temperature (www.adas.ac.uk).

Both recombination with the free electrons in the cold electron swarm [28] and electron transfers from collisions with cold clusters can effect the charge [19]. As is true in most of the cluster experiments, the focal waist (10–20 μm) is much smaller than the span of the supersonic cluster jet around the focus. So there is a reasonable ensemble of unirradiated clusters that the ions traverse through before reaching the detector. This is especially a dominant process in a free jet where cluster ensemble densities are relatively higher. Further, intense ionization in the focal volume also results in emission of electrons that would undergo collisions with these surrounding cold clusters and form a cold electron swarm [28] through which the ion traverse.

Table 1. Tabulation of the charge transfer cross section used in charge conversion computation of oxygen ions [29].

Reaction channel	cross section (10^{-16} cm^2)
$O^0 \rightarrow O^-$	0.02
$O^+ \rightarrow O^0$	6.81
$O^{2+} \rightarrow O^+$	1.97
$O^{3+} \rightarrow O^{2+}$	0.26
$O^{4+} \rightarrow O^{3+}$	0.27
$O^{5+} \rightarrow O^{4+}$	0.36
$O^{6+} \rightarrow O^{5+}$	0.33
$O^{7+} \rightarrow O^{6+}$	0.51
$O^{8+} \rightarrow O^{7+}$	0.48

In the two-step model, the charge reduction reactions along the traversal for oxygen ions are accounted for by the following coupled differential equations for $q = -1, 0, +1, \cdots, +8$:

$$\frac{dN_{O^q}(x)}{dx} = -\sigma_{e_{q,q-1}} N_{O^q}(x)[e] + \sigma_{e_{q+1,q}} N_{O^{q+1}}(x)[e] - \sum_{k<q} \sigma_{ct_{q,k}} N_{O^q}(x)[(CO_2)_n] + \sum_{j>q} \sigma_{ct_{j,q}} N_{O^j}(x)[(CO_2)_n], \quad (6)$$

where $[e]$ and $[(CO_2)_n]$ are electron and cluster densities, respectively, $N_{O^q}(x)$ is the number of O^q ions at the distance x, $\sigma_{e_{q,q-1}}$ is the effective cross section of ER reactions that reduce O^q to O^{q-1} and $\sigma_{ct_{q',q}}$ is the charge transfer cross section for reducing $O^{q'}$ to O^q $(q' > q)$ in collision with the CO_2 clusters. We measured the electron emission spectra of single-cluster nanoplasma and fitted it with a Maxwellian to determine the dominant cold electron temperature to be about 100 eV. Collisions in large cluster densities would reduce this temperature and to make the best case of ER we use $\sigma_{e_{q,q-1}}$ for an electron temperature of 1 eV (www.adas.ac.uk). This would give an upper limit on the contribution to charge reduction by ER. The charge transfer cross sections (CTCS) used in these calculations are given in table 1. The initial charge state propensity distribution $N_{O^q}(0)$ is obtained from the experimentally measured TP spectrum of single clusters (figure 2(a)). The cluster density and its variation along the jet span $[(CO_2)_n(x)]$ are measured using a calibrated pressure sensor. The electron density $[e]$ is inferred from the cluster density and the average number of electrons released per atom in the ionization of single clusters (estimated from the traces in figure 2(a)). For modeling equations for the negative ions, we include the collisional electron detachment channel $(A^- + M \rightarrow A)$ which has cross section $\sigma_{\mathrm{coll}_{-1,0}}$ comparable to that of electron attachment ($\sigma_{\mathrm{ct}_{0,-1}}$ [30]).

ER reactions have low cross sections and even at the best parameters used here (1 eV electron temperature that has the highest cross section), this process cannot account for transfer of population from high charge state to low charge states. With an $[e] \simeq 10^{18}$ cm^{-3}, a 2 cm traversal length (assuming that the electron swarm extends up to the jet span) and with $\sigma_{e_{q,q-1}} \sim 10^{-22}$–$10^{-24}$ cm^{-3} for the different charge states q, the fraction of the ions reduced by ER is only 10^{-4}–10^{-6}.

In general, the cross sections for charge transfer are higher than recombination reactions. Since the CTCS are not available in collisions with clusters, the CTCS measured for the

monomer species is to be appropriately scaled to account for the CTCS of clusters. It should also be noted that head-on collisions of an ion with a few nm clusters would lead to a large change in momentum and scatter the ion. Since we are sampling the ion signal in the TPS with a 200 μm extraction aperture at about 20 cm from interaction zone, head-on collisions are discriminated in the measurements. In view of this, the CTCS is scaled with the number of atoms on the periphery of the spherical cluster. We follow a formalism that has been used in the literature [31] and is proven to yield correctly scaled cross sections. If R is the cluster radius, and $\sigma_{\mathrm{ct,mono}}$ the CTCS of the monomer, then $\sigma_{\mathrm{cluster}} = 3/2 \times (\delta R/R)^2 \times N_C \times \sigma_{\mathrm{ct,mono}}$, where δR is the size of the monomer and N_C is the cluster size. The CTCS is also a function of the ion energy; however, in a 1–5 keV amu^{-1} energy range (the mean energy of the O^{q+} ions in our measurements is at most 40 keV) there is no significant change in the CTCS. Typically, with the CTCS for monomer species of about 10^{-16} cm^2, the CTCS scaled for clusters of 3–4 nm are about two orders of magnitude larger. This is similar to the increase in the measured cross sections for carbon clusters as compared to that of atomic systems [32].

Our calculations show that with cluster densities of about 8×10^{13} cm^{-3} on an average at most two electrons are transferred per atom and this results in only about 10% ions being reduced to neutral oxygen and less than 0.1% ions to negative ion. This is far too small to account for the charge reduction seen in our experiments (complete transfer of high charge state population to low charge states and O^- yield similar to O^+). Charge transfer as a mechanism does not even explain the unusual charge reduction of positive ions, let alone the formation and copious emission of the negative ions.

To understand this large discrepancy between measurements and calculations and to identify the actual mechanism which results in a large fraction of negative ions, we explore the role of the laser-heated electrons extraneous to the cluster ionization in the focal volume [33]. We revise the two-step model, that failed to explain the observations and introduce a third step. We invoke the formation of a sheath of excited clusters surrounding the focal volume by the collisional excitation of the electrons that stream out of focus. In the third step ions that encounter the Rydberg excited clusters undergo a very efficient charge transfer reaction.

The existence of an ionization front [34] in dense cluster ensembles is well known. Energetic electrons stream out of the focal volume and heat matter surrounding the focal volume. Ionization outside the focal volume by plasma electrons has been experimentally probed by interferograms in dense gas clusters [20]. Experiments on different clusters systems [1, 35] have shown that for intensities of about 10^{16} W cm^{-2} with 800 nm light of pulse durations 40–200 fs, the electrons energy spectrum is typically a two-temperature Maxwellian, where the lower temperature is about 100–400 eV and the high temperature is about 1.5–2 keV. The low-energy component with a large yield is optimum for the ionization of atoms and hence the increase of electron density outside the focal volume [20]. However, one important aspect that has been ignored so far is the electronic excitation of the clusters by electron impact. At an electron energy of say 100 eV, the cross section for ionization (1.1×10^{-16} cm^2) is comparable to the excitation cross section (0.8×10^{-16} cm^2) [36]. This would hence imply the presence of a large fraction of excited clusters. Also, ionization followed by recombination in a solid-density medium such as a cluster can also induce electronic excitation. Thus, in a dense cluster ensemble both direct excitation by electron impact and indirect excitations via recombination lead to the formation of electronically excited states in the region surrounding the focal zone. It should be noted that excitation to even Rydberg states of clusters is well proved in a number of electron impact experiments [37]. In fact, clusters have been identified as unique with regard to electronic

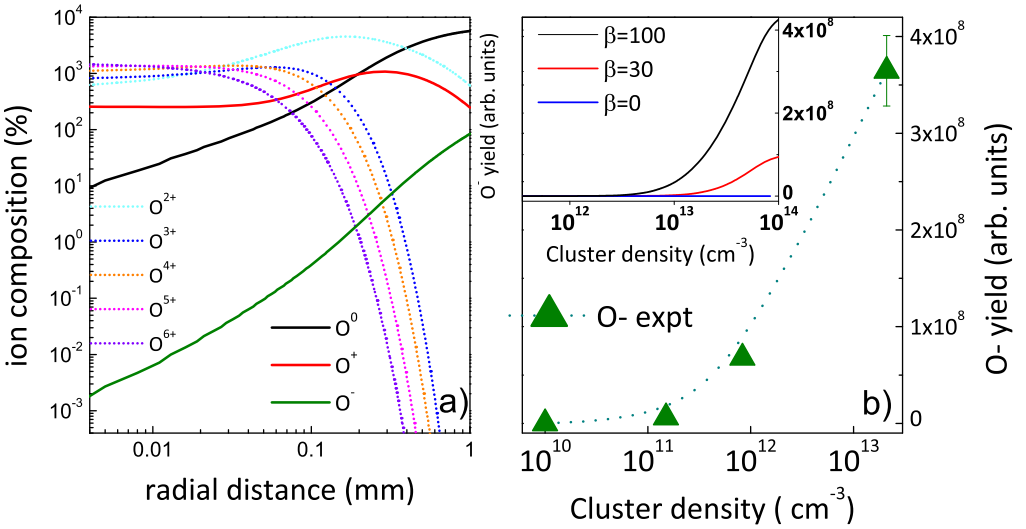

Figure 7. (a) Change in ion flux of a given charge as a function of the distance traversed through the cold cluster ensemble. A demonstrative representation of solutions to equation (7) for $\beta = 100$ is given. (b) O^- ion propensity measured at 2×10^{16} W cm^{-2} for different cluster densities. The dotted line is drawn to guide the eye. The inset shows the computed flux of the O^- ions for different values of excitation parameter β. Line with $\beta = 0$ implies charge reduction is only by normal charge transfer. $\beta = 100$ represents O^- yield when about 10% of the neighboring clusters are excited to $n \sim 6$.

excitations owing to their mesoscopic properties [38]. For an electron density of 5×10^{19} cm^{-3} and a cluster density of $\simeq 10^{14}$ cm^{-3}, given that there are about 10^5 atoms per cluster, the fraction of electronic excited atoms can be as large as 30% in the immediate neighborhood of the focal volume. This estimate relies on the energy deposition on the cold clusters by the streaming electrons from the focal volume using the cross sections for electron impact excitations [36]. Considering that in non-local heat transport experiments almost a 100% increase in electron densities outside the focal volume has been measured [20], this estimate is well justified.

The Rydberg excitations inherent in a densely clustered medium can thus explain the measured negative ion yield and its strong density dependance. The electronic excitations would change the charge transfer rate dramatically. It has been shown that if electrons are excited to the nth electronic state, the charge transfer cross section would scale as $\sim n^4$. An enhancement of 3–5 orders magnitude in CTCS has been demonstrated in many experiments [39] with electronically excited collisional systems. In the simulation, therefore, we include a β parameter to account for the enhanced CTCS due to the electronically excited atoms. We define $\beta = s \times n^4$, where s is the fraction of atoms excited to an average state n by electron impact. Accordingly, $\beta = 130$ represents a scenario with $s = 0.1$ (that is, 10% of the clusters are electronically excited) with an average principal quantum number of $n \sim 6$. Negative ion formation is insignificantly small when only normal charge transfer reactions are considered. Figure 7 shows the negative ion yield calculated by solving the coupled differential equations given in equation (1) to account for the negative ion formation at different cluster densities. In the inset of figure 7(b), the blue line with a legend $\beta = 0$ gives the O^- yield with only normal charge transfer

Table 2. Comparison of the experimentally measured O^-/O^+ propensity at a cluster density of $8 \times 10^{13}\,cm^{-3}$ with the computational results for different values of the excitation parameter, β (see the text).

β	O^-/O^+
0	0.01
30	0.04
100	0.86
Experiment	0.88

and ER. It is also clear from the figure 7(b) inset that only for $\beta > 0$ there is appreciable negative ion formation. It is more apt to compare relative ionization yields determined experimentally with the computations rather than the absolute O^- flux. We take the ratio of O^- and O^+ for a given energy in figure 6 and obtain the ratio that is averaged over the entire energy range. Although the ion detection efficiency changes a little with ion energy, the relative change for O^- and O^+ of a given energy is small and the correction in the energy averaged ratio is too little to influence the comparison with the computations. Table 2 gives a direct comparison of this ratio for the O^-/O^+ measured and also computed with different values of β. Calculations for two different values of β are shown along with that from the normal charge transfer ($\beta = 0$). As seen in figure 7 and the data presented in table 2, an intermediate value of $\beta = 30$ is inadequate to reproduce the experimental observation but $\beta = 100$ gives negative ion propensity comparable to the experiments. In figure 7(a), we show the change in ion signals computed from equation (7) for $\beta = 100$. From the numbers evaluated for electronic excitation, it is very reasonable that β can be about 100. Thus the negative ion formation and its unusually large yield, which is comparable to that of positive ions, can be comprehensively explained by enhanced charge transfer from electronically excited clusters.

In summary, we observe the emission of highly energetic negative ions as large as 300 keV from a densely clustered medium with a particle yield comparable to the positive ions. The origin of these negative ions is extraneous to the ionization of single nanoclusters and is attributed to highly efficient electron transfers from a sheath of Rydberg excited clusters around the focal volume. It is found that low-energy electrons emitted from the nanoclusters within focal volume are key to the formation of Rydberg excitations as well as the generation of negative ions. Our analysis reveals meagre negative ion counts sans these electronic excitations. Also, the negative ion yield strongly depends on the cluster density and the maximum O^- energy is a function of the cluster size. Our analysis comprehensively explains the generation of accelerated negative ions. Combining compact laser-based ion sources with conventional acceleration is being considered for many applications including medical diagnostics and cancer treatment [40]. The copious generation of accelerated negative ions shown in this work opens up the possibility of conceiving tandem acceleration schemes.

Acknowledgments

We thank E Krishnakumar for many insightful discussions. MK acknowledges support through a Swarnajayanti Fellowship from the Department of Science and Technology, Government of India.

References

[1] Fennel T *et al* 2010 Laser-driven nonlinear cluster dynamics *Rev. Mod. Phys.* **82** 1793

[2] Saalmann U, Siedschlag Ch and Rost J M 2006 Mechanisms of cluster ionization in strong laser pulses *J. Phys. B: At. Mol. Opt. Phys.* **39** R39

[3] Krainov V P and Smirnov M B 2002 Cluster beams in the super-intense femtosecond laser pulse *Phys. Rep.* **370** 237

[4] Protopapas M, Keitel C H and Knight P L 1997 Atomic physics with super-high intensity lasers *Rep. Prog. Phys.* **60** 389

[5] Augst S, Strickland D, Meyerhofer D, Chin S L and Eberly J H 1989 Tunneling ionization of noble gases in a high-intensity laser field *Phys. Rev. Lett.* **63** 2212–5

[6] Wilks S C and Kruer W L 1997 Absorption of ultrashort ultra-intense laser light by solids and overdense plasmas *IEEE J. Quantum Electron.* **33** 1954

[7] Mcpherson A, Thompson B D, Borisov A B, Boyer K and Rhodes C K 1994 Multiphoton-induced x-ray emission at 4–5 keV from Xe atoms with multiple core vacancies *Nature* **370** 631–4

[8] Rajeev R, Rishad K P M, Madhu Trivikram T, Narayanan V, Brabec T and Krishnamurthy M 2012 Decrypting the charge-resolved kinetic-energy spectrum in the Coulomb explosion of argon clusters *Phys. Rev.* A **85** 023201

[9] Ditmire T *et al* 1997 High-energy ions produced in explosions of superheated atomic clusters *Nature* **386** 54–6

[10] Smith R A and Ditmire T 2001 Interactions of intense laser beams with extended cluster media *Molecules and Clusters in Intense Laser Fields* ed J Posthumus (Cambridge: Cambridge University Press) pp 216–57

[11] Rajeev R, Rishad K P M, Madhu Trivikram T, Narayanan V, Brabec T and Krishnamurthy M A 2012 Thomson parabola ion imaging spectrometer designed to probe relativistic intensity ionization dynamics of nanoclusters *Rev. Sci. Instrum.* **82** 083303

[12] Peltza C and Fennel T 2010 Resonant charging of Xe clusters in helium nanodroplets under intense laser fields *Eur. Phys. J.* D **63** 281–8

[13] Krainov V P and Sofronov A V 2006 Recombination processes in atomic clusters irradiated by superintense femtosecond laser pulses *JETP* **103** 35–8

[14] Kumarappan V, Krishnamurthy M and Mathur D 2001 Asymmetric high-energy ion emission from argon clusters in intense laser fields *Phys. Rev. Lett.* **87** 085005

[15] Deiss C, Rohringer N, Burgdörfer J, Lamour E, Prigent C, Rozet J-P and Vernhet D 2006 Laser–cluster interaction: x-ray production by short laser pulses *Phys. Rev. Lett.* **96** 013203

[16] Ditmire T, Zweiback J, Yanovsky V P, Cowan T E, Hays G and Wharton K B 1999 Nuclear fusion from explosions of femtosecond laser-heated deuterium clusters *Nature* **398** 489–92

[17] Ditmire T, Donnelly T, Falcone R W and Perry M D 1995 Strong x-ray emission from hot plasmas produced by intense irradiation of clusters *Phys. Rev. Lett.* **75** 3122

[18] Nakamura T *et al* 2009 High energy negative ion generation by Coulomb implosion mechanism *Phys. Plasmas* **16** 113106

[19] Ter-Avetisyan S 2011 MeV negative ion generation from ultra-intense laser interaction with a water spray *Appl. Phys. Lett.* **99** 051501

[20] Ditmire T, Gumbrell E T, Smith R A, Djaoui A and Hutchinson M H R 1998 Time-resolved study of nonlocal electron heat transport in high temperature plasmas *Phys. Rev. Lett.* **80** 720–3

[21] Kumarappan V, Krishnamurthy M, Mathur D and Tribedi L C 2001 Effect of laser polarization on x-ray emission from Arn ($n = 20010^4$) clusters in intense laser fields *Phys. Rev.* A **63** 023203

[22] Hagena O F 1992 Cluster ion sources *Rev. Sci. Instrum.* **63** 2374

[23] Arefiev A V *et al* 2010 Size distribution and mass fraction of microclusters in laser-irradiated plasmas *High Energy Density Phys.* **6** 121–7

[24] Weast R C (ed) 1981 *CRC Handbook of Chemistry and Physics* 62nd edn (Boca Raton, FL: CRC Press)

[25] Krishnamurthy M, Mathur D and Kumarappan V 2004 Anisotropic charge-flipping acceleration of highly charged ions from clusters in strong optical fields *Phys. Rev.* A **69** 033202
[26] Christophorou L G and Stockdale J A D 1956 Dissociative electron attachment to molecules *J. Chem. Phys.* **48** 1956
[27] Krishnakumar E, Kumar S V K, Rangwala S A and Mitra S K 1997 Dissociative-attachment cross sections for excited and ground electronic states of SO_2 *Phys. Rev.* A **56** 1945–53
[28] Ditmire T, Donnelly T, Rubenchik A M, Falcone R W and Perry M D 1996 Interaction of intense laser pulses with atomic clusters *Phys. Rev.* A **53** 3379–402
[29] Phaneuf R A, Janev R K and Pindzola M S (ed) 1987 *Atomic Data for Fusion. Volume 5: Collisions of Carbon and Oxygen Ions with Electrons H H_2 and He* ORNL-6090
[30] Ishii K, Tanabe T, Lomsadze R and Okuno K 2001 Charge-changing cross sections in collisions of C^{q+} ($q = 2$–5) with He and H_2 at energies below 750 eV u^{-1} *Phys. Scr.* **T92** 332
[31] Tappe W, Flesch R and Ruhl E 2002 Charge localization in collision-induced multiple ionization of van der Waals clusters with highly charged ions *Phys. Rev. Lett.* **88** 143401
[32] Martin S *et al* 2006 High formation yields of negative ions in multicharged fluorine F^{q+} ($q = 1$–3)-C_{60} collisions *Europhys. Lett.* **74** 985
[33] Rajeev R, Madhu Trivikram T, Rishad K P M, Narayanan V, Krishnakumar E and Krishnamurthy M A 2013 compact laser-driven plasma accelerator for megaelectronvolt-energy neutral atoms *Nature Phys.* **9** 185
[34] Edwards M J *et al* 2001 Investigation of ultrafast laser driven radiative blast waves *Phys. Rev. Lett.* **87** 085004
[35] Kumarappan V, Krishnamurthy M and Mathur D 2003 Asymmetric emission of high-energy electrons in the two-dimensional hydrodynamic expansion of large xenon clusters irradiated by intense laser fields *Phys. Rev.* A **67** 043204
[36] Raju G 2004 Electron-atom collision cross sections in argon: an analysis and comments *IEEE Trans. Dielectr. Electr. Insul.* **11** 649
[37] Bondarenko E A *et al* 1991 New emission continua of rare-gas clusters in the VUV region *Chem. Phys. Lett.* **182** 637
[38] Sisourat N *et al* 2010 Ultralong-range energy transfer by interatomic Coulombic decay in an extreme quantum system *Nature Phys.* **6** 508–11
[39] Olson R E 1980 Ion-Rydberg atom collision cross sections *J. Phys. B: At. Mol. Phys.* **13** 483–92
[40] Krushelnick K *et al* 2000 Ultra high intensity laser-produced plasmas as a, compact heavy ion injection source *IEEE Trans. Plasma Sci.* **28** 1110–5